http://doi.org/10.29227/IM-2021-02-04 Received: 15 Aug 2021, Accepted: 25 Sep 2021, Published: 10 Nov 2021

Mining-induced Land Subsidence Detected by Sentinel-1 SAR Images: An Example from the Historical Tadeusz Kościuszko Salt Mine at Wapno, Greater Poland Voivodeship, Poland

KIM Thi Thu Huong[1, 2, *], TRAN Hong Ha[2, 3], BUI Khac Luyen[2], LIPECKI Tomasz[1]

[1] AGH University of Science and Technology, Kraków, Poland

[2] Hanoi University of Mining and Geology, 18 Vien street, Hanoi, Vietnam

[3] Institute of Geo-Engineering, Clausthal University of Technology, Clausthal, Germany

Corresponding author: huongktt87@gmail.com

Abstract. There are many mines in Poland that have been in operation for over 100 years, with the Tadeusz Kościuszko mine being a large salt mine in Wapno, northern Poland. The mine was closed in 1977 due to the greatest catastrophe in the history of Polish mining, but in the first days of 2021, a very large hole has been created in this area due to land subsidence. This article uses InSAR technology with Sentinel-1 images to determine settlement and ongoing deformation in this mine. The study results are useful for policymakers, managers, and authorities because land subsidence has caused serious and dangerous effects on people living in the area. The results processed by the Persistent Scatterer InSAR (PSInSAR) method with the Sentinel Application Platform and the Stanford Method for Persistent Scatterers software packages show that deformation in the Wapno village area has been detected in both residential and non-residential areas, with maximum subsidence of up to −19 mm/yr. The subsidence in the mine reaches −12 mm/yr, and that at surrounding area range from 0 to −18.8 mm/yr.

Keywords: PSInSAR, Land subsidence, Mining, Wapno, Poland

1. Introduction

Poland is the biggest mining country in Europe, of which mineral mines concentrate in half of the country, stretching from North-West to South-East (see Fig. 1). Many of them are over 100-year-old excavation mines. As a result, mining-induced land surface deformation is happening, attracting much scientific research in the country.

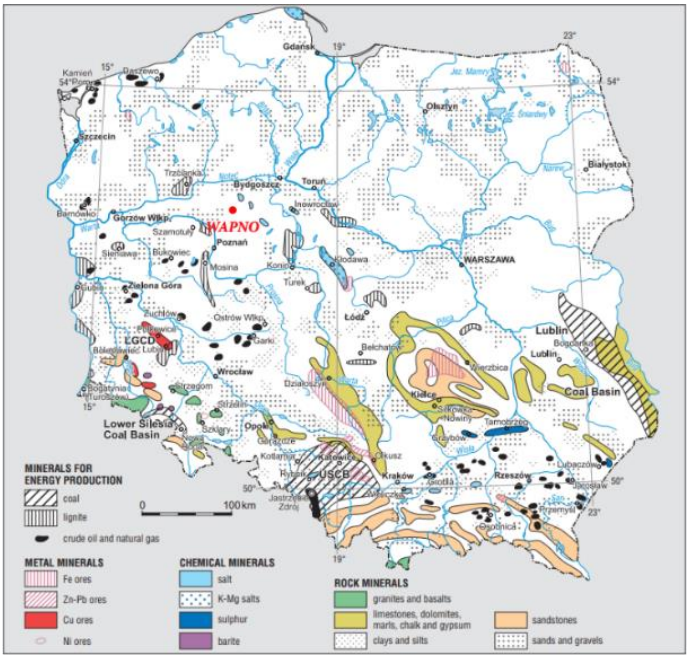

Fig. 1. Distribution of mineral mines in Poland adapted from Kowalczyk Andrzej, Witkowski Andrzej [1]. The red dot is the study area of Wapno, Wielkopolskie, Poland.

Tadeusz Kościuszko is a well-known rock salt mine in Poland, which is located in Wapno, northern Poland. In 1977, the most terrible disaster in the mining history of Poland had happened in this mine, that

a sudden increase of groundwater flooded a level of the mine and broke the insulation layer. A huge sinkhole with a depth of several meters has been created in the village on 28th October 1977. Consequently, 40 buildings were destroyed, and trees, roads, and railway tracks disappeared into the abyss. About 1400 residents had to evacuate, among which some of them have left the village forever. Many years later, the subsidence and appearance of the sinkholes still happened. Other smaller sinkholes also happened in 2007 and 2017. On 26th February 2021, a big sinkhole appeared in the area of the old mine. The risk of ground subsidence is subject to happen at any time [2]. It was shown that from October 2014 to June 2020, the subsiding rate increased from 3 millimeters per year (mm/yr) to 8 mm/yr [3]. Ground deformation in and around an underground mining area frequently occurs. It is a major component of the displacement vector, triggered by underground mining [4]. In Poland, mining-induced land subsidence has been measured by conventional methods, such as geodetic leveling, total stations, or the Global Navigation Satellite System (GNSS). In recent years, it has also been measured by other methods, including Interferometric Synthetic Aperture Radar (InSAR), Unmanned aerial vehicle (UAV), or laser scanning. Conventional methods are labor-intensive and time-consuming [5]. Additionally, these techniques gather data on a point-by-point basis with limited spatial coverage, which does not provide enough information about the whole surface subsidence. Therefore, the monitoring is usually limited to small areas. InSAR, UAV, and laser scanning, in contrast, allow monitoring land surfaces in very large areas with a very high number of measured points. Hence, these technologies are applied more and more in both the science and industry sectors.

Differential InSAR (DInSAR) is a technique in which two SAR scenes acquired over the same area on the Earth, but at different acquired times, are used to derive the Earth's surface deformation [4]. In DInSAR, the contribution of topography is removed from the phase change between the two SAR scenes. It can be used to quantify a small displacement of the land surface [6]. However, the results of DInSAR are affected by the various error and noise sources, e.g., atmospheric artifact, topographical and orbital errors. Therefore, different multi-temporal InSAR (MTInSAR) methods have been proposed, which exploit a big SAR dataset. Small baseline subset (SBAS) [7] and Persistent Scatterer InSAR (PSInSAR) [8] are among the most commonly used MT-InSAR methods [9]. While PSInSAR optimizes pixels with single scatterers, SBAS optimizes those with distributed scatterers [10]. Additionally, SBAS is advantageous in that redundant interferograms can be adopted to reduce noise, particularly in areas of low deformation magnitude affected by high noise [11]. In contrast, in PSInSAR, all interferograms are generated to a single primary, which allows for noise reduction of the primary image as it exists in all interferograms [12].

The PSInSAR method has been employed in the literature worldwide in monitoring Earth's surface deformation, which is associated with groundwater extraction and urbanization[12], mine exploitation [13], [14] among others. In Poland, the first application of PSInSAR for displacement monitoring was published in 1998 by Perski [15] in The Silesian coal mine region. Since then, Zbigniew Perski and his partners started publishing their studies on using InSAR for many areas in Poland: application of satellite radar interferometry in the areas of copper ore mining in LGOM [16], for surface deformation monitoring in the urbanized area of Malbork, northern Poland [17]; analysis of terrain deformation near the Wieliczka salt mine [18] and Nowy Sącz [19]. In 2006, Marek Graniczny and his partners published their article using PSInSAR in observing displacement in the Mining of Silesia Region, Poland [20].

Mapping ground vertical movement caused by salt mining activities with the Sentinel-1 Terrain Observation with Progressive Scanning (TOPS) data was performed by Malinowska, Hejmanowski [21], which was applied to the Wieliczka salt mine in the years 2015-2016. The results have shown the subsidence dynamics in the western part of the Wieliczka town of up to 20 mm/year. Smaller subsidence was observed in the eastern part of the town, not exceed 10 mm/year [21]. Deformation around the Wieliczka salt mine was also studied by [18] and Mirek [22].

However, InSAR has not been employed in the Tadeusz Kościuszko salt mine to date. This study shows the application of InSAR in monitoring the land deformation in the Tadeusz Kościuszko salt mine over the one-year period, between March 2020 and March 2021. The objective of the study is to demonstrate the possibility of the application of the PSInSAR method with Sentinel-1 SAR data to quantify surface deformation around this ancient salt mine and in the Wapno village.

The remainder of the paper is structured as follows: Section 2 introduces the history of the Tadeusz Kościuszko salt mine in Wapno, Grater Poland Region, Poland. In Section 3, the study area, materials, and method are provided. Section 4 provides experimental results, and Section 5 concludes the study.

2. History of the Tadeusz Kościuszko salt mine Wapno, Greater Poland Voivodeship, Poland

Wapno is a large village in west-northern Poland. In 1828, the header of the Wapno village began exploiting the gypsum open-pit mine, which laid shallow under the ground. Then, they realized that there was a big salt layer covered with a gypsum – clay cap with a thickness of 20–160 m. In 1898, the permit for the operation was bought by the German Company Solwerke. In 1910, the drilling of the Wapno I–a mining shaft, was started at 101.5 m depth – due to the enormous inflow of water – this work was stopped. Therefore, during 1912–1917, the Wapno II shaft was exploited. It was reached 420 m underground in 1916. From May 1917 to June 1918, at a depth of 406 m – the first level of mine (later, it is level IV), 450 m main working in the mine was drilled. Then, more four parallel exploded ways in the mine were also drilled. The next levels were created over time according to the depth: 345 m (level I), 365 m (level II), 385 m (level III), 430 m (level V), and 455.5 m (level VI). The salt mine was exploited to level XII at a depth of 648 m and, in the middle of 1960-years, even prepared for the construction of levels VIII and IX [23]. The Wapno salt mine is in the area of 1000×350 m. The salt-mining exploitation was started at level IV. The excavated material was transported to the ground by a steam hoisting machine and a wooden pane tower. Both were replaced in 1930 – 1931 by a modern type of steam hoisting and a steal double-shot over shaft tower. All factory was already electrified at that time, achieved in the 1920s more and more output products - growing from 17234 tons in 1920 to 86422 tons in 1925 (42,1 % of all salt excavation in Poland at that time), and the company's best result in the entire war period – 100 896 tons salt in 1930 [23].

In 1956, the name of the company was established as the Tadeusz Kościuszko salt mine. From 1950 to 1965, the production of the mine accounted for more than half of the rock salt extracted in Poland during this time. During 1967−1975, the annual production of salt exceeded 400 thousand tons. It was exported to Czechoslovakia, Hungary, Sweeden, Finland, Norway, Guinea, Great Britain, Denmark, Nigeria. In the 1970s, the mine's water hazard increased due to the existence of a very thin layer, which separated the deposit from the water in the overburden formation. In 1976, water leakage into the working place was detected. On 5th August 1977, one of the greatest catastrophes in the history of Polish mining occurred in the mine, that a sudden increase of groundwater flooded the third level. The main causes were the creation of hydraulic connections between the excavation [23-24].

On 28th October 1977, a huge sinkhole appeared in the village, by which over 40 buildings were destroyed while trees, roads, and railway tracks disappeared into the abyss [2]. The Wapno village was inaccessible for about two years between 1978 and 1979. Around 1400 residents were evacuated from the village, many of them left their place forever. As a result of the mining catastrophe, Wapno has lost about half of its inhabitants. According to the data published in December 2018, there were 1650 people living in the village [25]. The financial losses caused by this catastrophe have not been counted. Wapno has never regained its prosperity in the 44 years from 1977 to 2021 that have passed since the disaster. Today, in the mining disaster areas, Obrońcy Stalingradu Ogrodowa, Staszic, and Świerczewski streets do not exist anymore, and the forest has grown instead [25]. Fig. 2 shows examples of typical land subsidence-induced damages in the Wapno village.

Fig. 2. (left) Garages in Karol Swierczewski Street were completely collapsed by a huge sinkhole on 5th August 1977, (middle) railway tracks were broken in the Wapno village [25], (right) A huge hole in the Wapno village, which was allegedly caused by land subsidence triggered by mining exploration in the Tadeusz Kościuszko salt mine [26].

3. Study area, dataset, and method

3.1. Study area and dataset

The study area is located in the northern part of Poland, over the area of the ancient Tadeusz Kościuszko salt mine in the Wapno village, which is located in Gmina Wapno (see Fig. 3, left). Wapno means lime in the Polish language, in which there are large gypsum and lime deposits. There are also large deposits of rock salt, which were started to be excavated from the beginning of the nineteenth century. In addition, Wapno is close to several lakes and thus is called Gniezno Lake District. The study area is limited from $52^0$52' N to $52^0$58'N and $17^0$21'2.52" E to $17^0$35'54.96" E (see Fig. 3, right). It covers all the Wapno village. The Tadeusz Kościuszko salt mine was closed, but people are still living around with kindergarten, primary school, church, post office, grocery store, buildings, and houses.

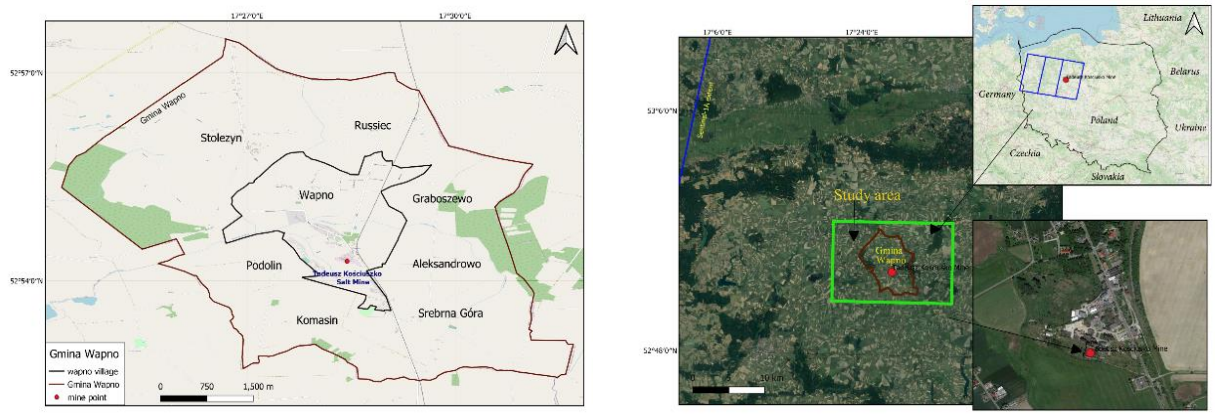

Fig. 3. (left) Location of the Wapno village with the red dot indicating the Tadeusz Kościuszko Salt Mine, (right) The study area (green box). The extent of the Sentinel-1A data sub-swaths is indicated by blue boxes in the right panel. Red dots are the Tadeusz Kościuszko Salt Mine.

In this study, the Sentinel-1A data in the Single Look Complex (SLC) format are utilized. These data can be freely obtained from http://www.scihub.copernicus.eu. The dataset is acquired in the descending orbit number 22 and is processed in the Interferometric Wide-swath (IW) mode. We use a total of 32 images covering the 1-year time period, between March 9, 2020, and March 16, 2021, with a 12-day temporal interval. The radar wavelength of Sentinel-1 is ~5.55 cm, which corresponds to the C-band in the microwave spectrum. Tab. 1 shows the information of 32 images with the date of acquisition, perpendicular baseline, and temporal baseline. The image captured on September 29, 2020, was chosen as the primary image. Perpendicular baseline is the spatial distance between the first and secondary observations measured perpendicular to the look direction (means data from the primary and secondary images). It provides an indication of the sensitivity to terrain height, the degree of correlation due to phase gradients, and the effectiveness of the phase unwrapping. Temporal baseline is the time period between two dates of primary and secondary images acquisition.

3.2. Method

The Sentinel-1A data is processed with the PSInSAR method. The interferograms are formed with the image acquired on September 29, 2020, chosen as the primary image (see Tab. 1). The interferogram network is shown in Fig. **4**, in which image acquisition times are described along the X-axis, and perpendicular baseline lengths are indicated along the Y-axis. The number shown in the figure for each image indicates the perpendicular baseline w.r.t the primary image. The steps of data processing utilized in this study are shown in Fig. **5**. The interferograms are first processed by the Sentinel Application Platform (SNAP) software package by European Space Agency (ESA), then the InSAR time series are analyzed by the Stanford Method for Persistent Scatterers (StaMPS) software package [27]. These steps are described in Tab. **2**.

Tab. 1. List of Sentinel-1 SAR scenes used in this study. The image captured on September 29, 2020, is chosen as the primary image.

No	Date of acquisition	Perpendicular baseline (m)	Temporal baseline (days)
1	09 March 2020	100.85	204
2	21 March 2020	40.90	192
3	02 April 2020	-72.80	180
4	14 April 2020	-96.73	168
5	26 April 2020	-23.34	156
6	8 May 2020	-35.85	144
7	20 May 2020	23.31	132
8	1 June 2020	-75.18	120
9	13 June 2020	-41.17	108
10	25 June 2020	-34.47	96
11	07 July 2020	-19.42	84
12	19 July 2020	21.38	72
13	31 July 2020	43.82	60
14	12 August 2020	-73.89	48
15	24 August 2020	-51.59	36
16	05 September 2020	17.96	24
17	17 September 2020	47.80	12
18	29 September 2020	0	0
19	11 October 2020	-24.23	-12
20	23 October 2020	-61.16	-24
21	04 November 2020	43.39	-36
22	16 November 2020	60.71	-48
23	28 November 2020	2.31	-60
24	10 December 2020	-33.10	-72
25	22 December 2020	-31.88	-84
26	3 January 2021	34.62	-96
27	15 January 2021	72.77	-108
28	27 January 2021	97.71	-120
29	08 February 2021	49.32	-132
30	20 February 2021	-87.29	-144
31	04 March 2021	-98.05	-156
32	16 March 2021	-32.23	-168

http://doi.org/10.29227/IM-2021-02-04 Received: 15 Aug 2021, Accepted: 25 Sep 2021, Published: 10 Nov 2021

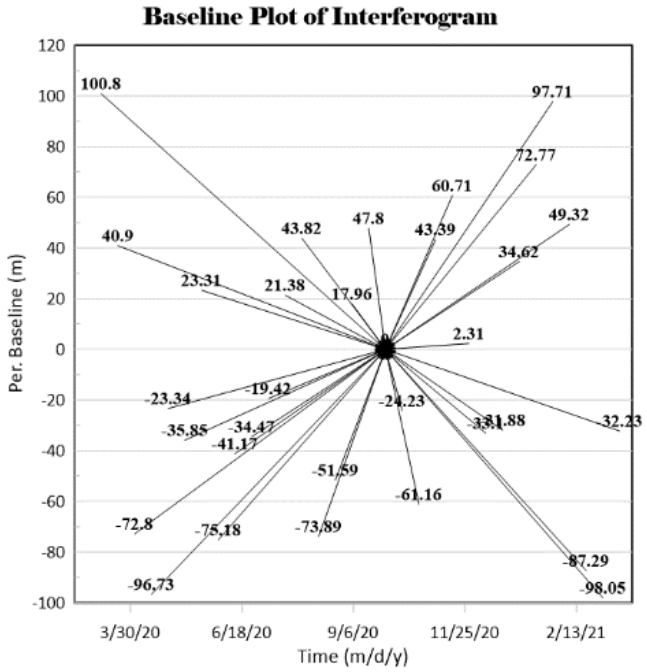

Fig. 4. The interferogram network with the primary image was acquired on September 29, 2020 (black dot).

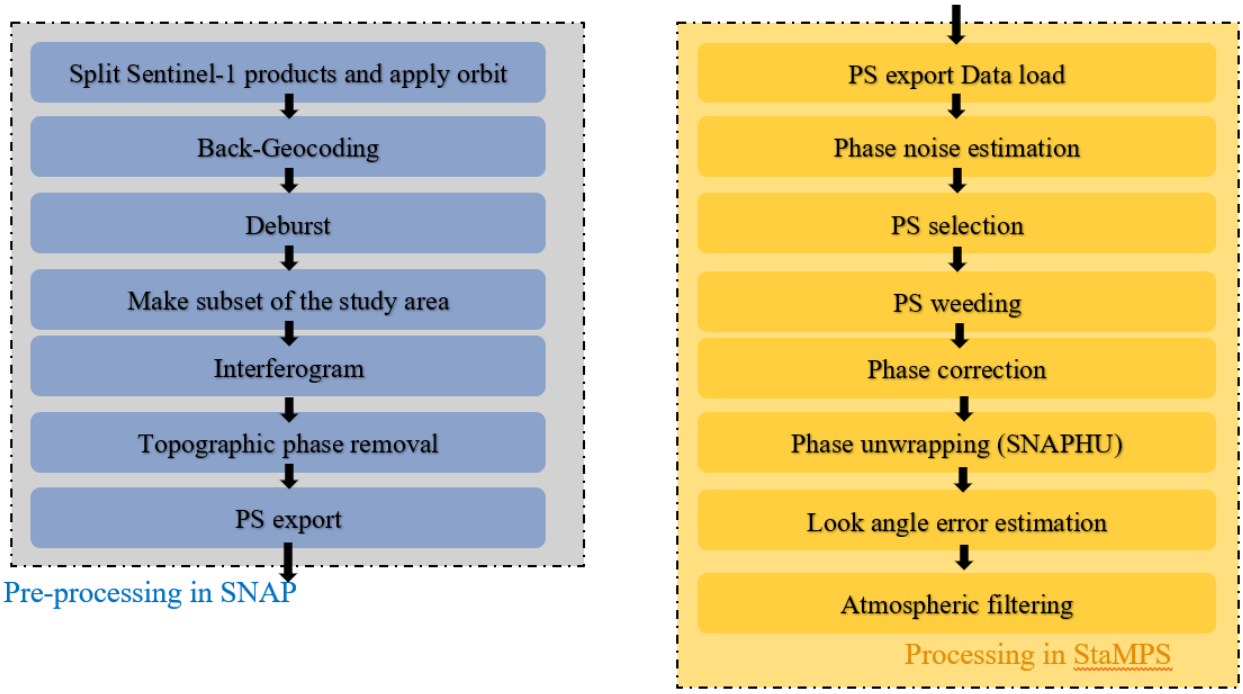

Fig. 5. Workflow of the PSInSAR data processing applied in this study: (left) Steps of interferogram formation by the SNAP software package and (right) PSInSAR time series analysis by the StaMPS software package.

Tab. 2. Description of the main processing steps by the PSInSAR method with the SNAP and StaMPS software packages.

No	Step	Description
1	Split Sentinel-1 products and apply orbit	Split Sentinel-1A images with the selected sub-swath, bursts, and polarization. Based on the accurate information of satellite position and velocity, the orbit state vectors in the metadata of the products are updated.
2	Co-registration	Co-registration of one or more slave images with a master on the same sub-swath using the orbit of the products and the digital elevation model.
3	Deburst	Merging of adjacent bursts in the azimuth direction according to their zero. Remove black path between bursts.
4	Subset	Make a subset to focus on the study area.
5	Interferogram	Form the interferograms.
6	Topographic phase removal	Remove phase due to topography.
7	StaMPS export	Export products to be subsequently processed in StaMPS.
8	Data load	Import the data from SNAP to StaMPS. Save the data in the MATLAB workspaces.
9	Phase noise estimation	Estimation of the phase noise value for each pixel in the interferograms.
10	PS selection	Selection of eligible PS pixel on a noise characteristics basis.
11	PS weeding	Remove PS noise or PS affected by signal contribution from neighboring elements.
12	Phase correction	Correction of the wrapped phase.
13	Phase unwrapping	Phase unwrapping by the SNAPHU method [28].
13	Look angle error estimation	Computation of spatially correlated look angle error
14	Atmospheric filtering	Exploiting triangle mesh generator and Delaunay triangulator.

4. Results

A total of 74 446 points have been generated from the data processing. These points are received from the backscatter of the satellite signal. There are low coherence points located in rural areas but high coherence points in constructions and buildings. Therefore, a coherence threshold of 0.4 is used to filter these low coherence points, by which 9 349 PS points are retained. The deformation rates for the entire study area are shown in Fig. **6**b. In this study, positive deformation reveals the movement of the Earth's surface toward the satellite (i.e., uplift), while negative deformation represents the movement away from the satellite (i.e., subsidence). Both indicate the movement along the vertical direction, which is converted from the line of sight (LOS) direction with an assumption that the horizontal component is insignificant by [12]:

$$d_U = \frac{d_{LOS}}{cos\theta_{inc}}$$

where d_U and d_{LOS} are the deformation in the vertical and LOS directions, θ_{inc} is the radar incidence angle.

No reference area is applied due to no evidence of a stable area (i.e., an area with a low deformation rate); thus, the deformation at detected points have been identified relative to the average deformation of the entire study area. As a result, both subsidence and uplift of the same maximum magnitude (i.e., ±30 mm/yr) are found in the study area. In the Wapno village, uplift and subsidence spread evenly over the area, as shown in Fig. **6**b. In the Wapno village, points of high subsidence (up to −19 mm/yr) are marked by red

dots in Fig. **6**b, which are located in non-residential areas (see Fig. 6a). They are distributed in the northern, central, and southern parts of the village marked by blue borders. In residential areas shown by the red borders, the subsidence between 0 and −8.6 mm/yr is found. In the salt mine area, most of the subsidence rates range from 0 to −9 mm/yr, with some points reaching −12 mm/yr.

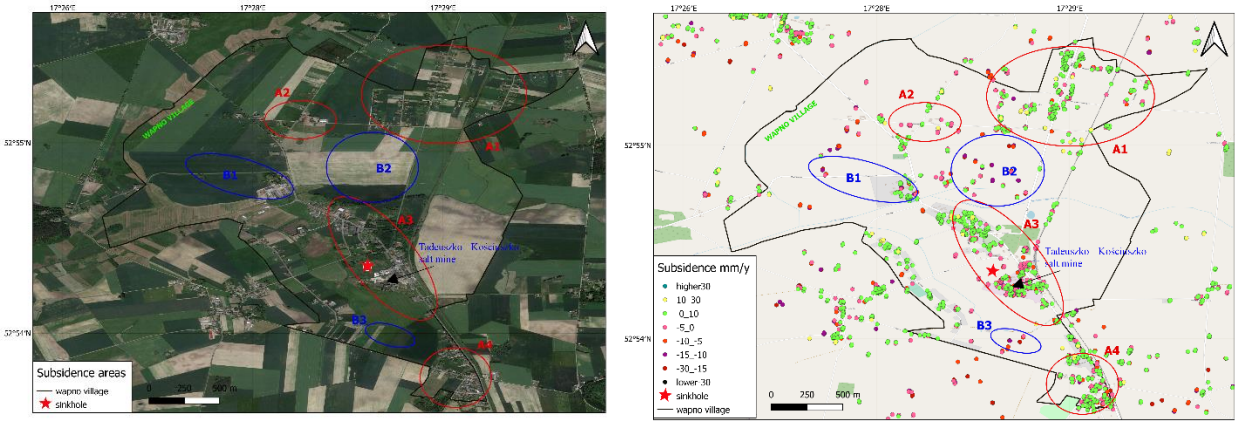

(a) (b)

Fig. 6. The deformation rates for the study area between March 9th 2020 and March 16th 2021. The big red star is the sinkhole, which appeared on February 26th 2021.

In each residential or non-residential area with the border shown in Fig. **6**, we extract points with the highest subsidence, which are shown in Fig. **7** and

Tab. **3**. It is shown that subsidence rates range between ~−15 mm/yr and ~−19 mm/yr in non-residential areas (P1 to P9), and ~−5.5 mm/yr and ~−14.5 mm/yr in residential areas (P10 to P16).

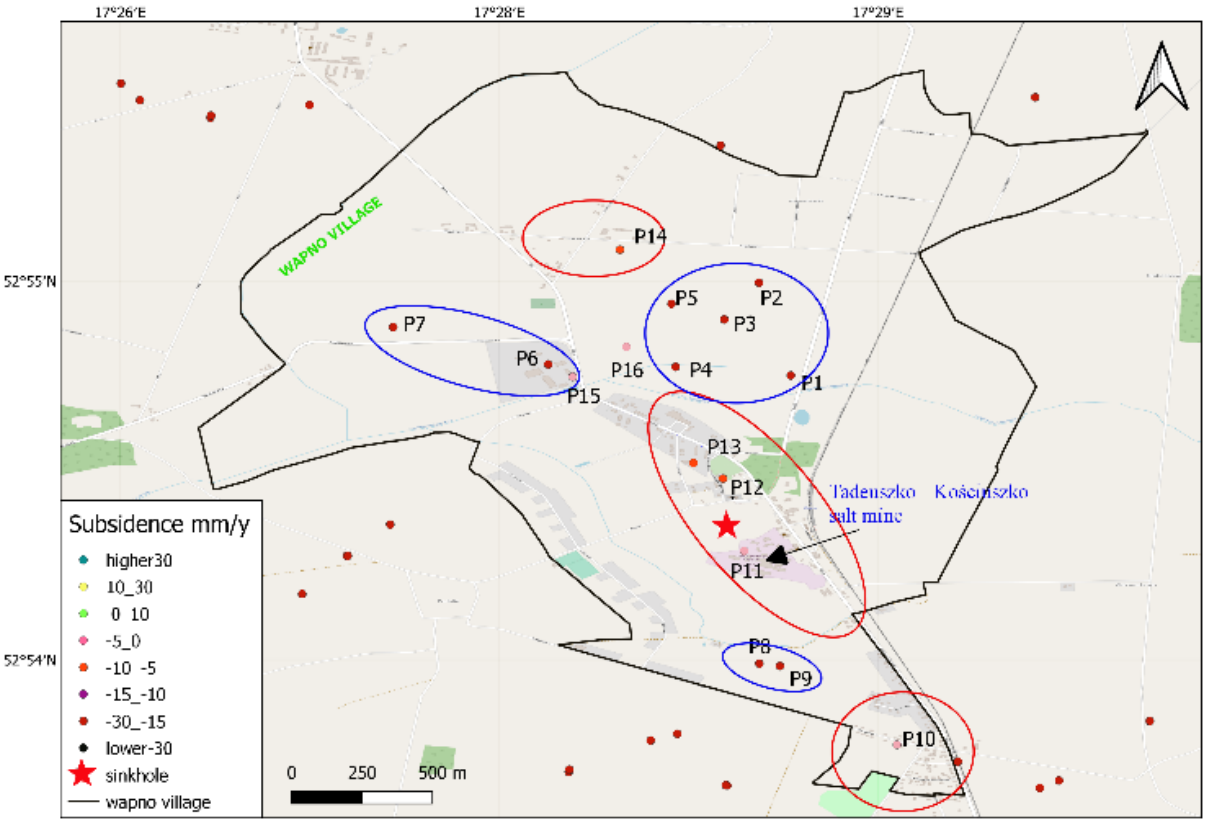

Fig. 7. Points of high subsidence rates were extracted for residential and non-residential areas.

Tab. 3. Coordinates and subsidence rates of high-subsiding points.

No	Points	Latitude (rad)	Longtitude (rad)	Subsidence (mm/y)
1	P1	52.91501	17.47541	-19
2	P2	52.91991	17.47373	-17.5
3	P3	52.91796	17.4719	-17.3
4	P4	52.91546	17.46933	-17.9
5	P5	52.91879	17.46911	-15.9
6	P6	52.9156	17.4626	-16.7
7	P7	52.91756	17.45442	-15.3
8	P8	52.8998	17.47375	-18.8
9	P9	52.89967	17.47484	-16.6
10	P10	52.89552	17.48102	-12.1
11	P11	52.90575	17.47295	-12.1
12	P12	52.90957	17.47183	-7
13	P13	52.91039	17.47027	-5.5
14	P14	52.92165	17.46639	-5.6
15	P15	52.91494	17.46389	-13.7
16	P16	52.91652	17.46673	-14.5

Ground deformation around the Tadeusz Kościuszko salt mine is shown in Fig. **8**. The maximum subsidence has occurred not only within the mine but also in surrounding areas (A, B, C in Fig. 8). There is a subsidence point with the rate of up to −18 mm/yr on the vacant lot (the southwest of the mine) (area C). As shown in Fig. **8**, there is not a special region with high deformation. The subsidence has happened in the entire Wapno village, including the Tadeuszko Kościuszko mine area. We see that the whole region of the Wapno village is under the same risk of land subsidence.

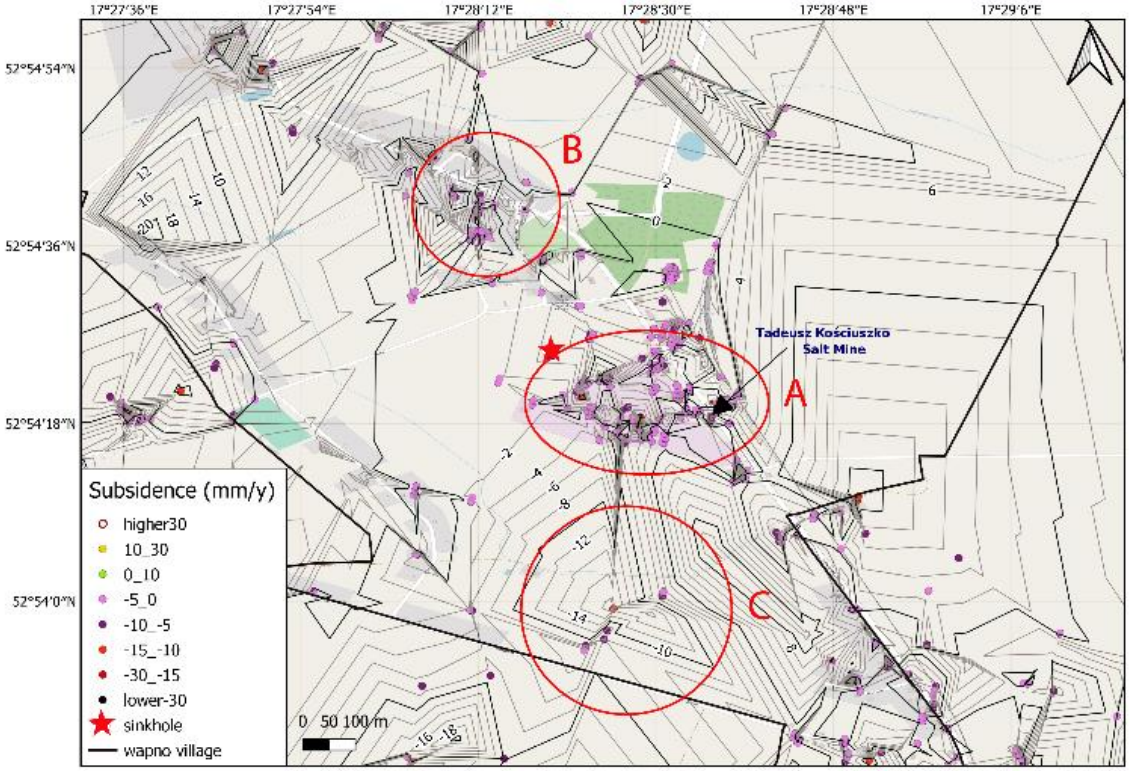

Fig. 8. Contour map of land subsidence in the Wapno village. The red star is the sinkhole, which happened on February 26th 2021.

5. Conclusions

With 32 Sentinel-1B SAR images collected between 9th March 2020 and 16th March 2021, the PSInSAR method was processed by the SNAP and StaMPS software packages to detect surface deformation in the historical Tadeusz Kościuszko salt mine and the surrounding area of Wapno, Poland. The results have shown that:

Sentinel-1 SAR data can be utilized with the PSInSAR method to detect deformation triggered by mining activities in the historical Tadeusz Kościuszko salt mine. Sentinel-1 SAR images, which are free with a regular acquisition interval of 12 days and a large spatial coverage compared to other SAR data, are advantageous.

In this study, deformation in the Wapno village area has been detected with maximum subsidence of up to −19 mm/yr, and the inactive Tadeusz Kościusko experienced subsidence in most of its area. Subsidence in this mine reach −12 mm/yr and that at surrounding area ranged from 0 to −18.8 mm/yr.

Land deformation has been reported in this study from Sentinel-1 SAR application, but no validation relying on individual measurements, e.g., GNSS or total station data, was conducted. Though the application of PSInSAR and the Sentinel-1 SAR data has been proved to have accurate results of deformation, InSAR measurements are affected by different noise sources, which vary between study areas. Therefore, the confidence of the accuracy of InSAR-derived deformation in the study area should further be validated.

6. Acknowledgments

The paper was presented during the 6th VIET - POL International Conference on Scientific-Research Cooperation between Vietnam and Poland, 10-14.11.2021, HUMG, Hanoi, Vietnam.

7. References

1. Kowalczyk Andrzej, Witkowski Andrzej, Różkowski Andrzej, Szczepański Andrzej, Rogoż Marek, Przybyłek Jan, and S. Stanisław., 2010; What Polish mining owes to Polish hydrogeology, 58; 9/1; 774-786.

2. https://www.abandonedspaces.com/uncategorized/salt.html; 2020 Makeenko, V.; The Salt Mine, Which destroyed a Village in 1977.

3. https://www.pgi.gov.pl/osuwiska/sopo-aktualnosci/szczegoly/12833-sol-niszczy-wapno-zapadlisko-nad-stara-kopalnia.html; 2/3/2021 Geozagrożeń, z.C.; Sól niszczy Wapno – zapadlisko nad starą kopalnią.

4. Pawluszek-Filipiak, K. and A.J.E.J.o.R.S. Borkowski, 2021; Monitoring mining-induced subsidence by integrating differential radar interferometry and persistent scatterer techniques, 54; sup1; 18-30.

5. Jung Hahn Chul, Kim Sang-Wan, Jung Hyung-Sup, M.K. Duck, and W. Joong-Sun, 2007; Satellite observation of coal mining subsidence by persistent scatterer analysis, Engineering Geology; 92; 1-2; 1-13.

6. Wempen, J.M.J.I.J.o.M.S. and Technology, 2020; Application of DInSAR for short period monitoring of initial subsidence due to longwall mining in the mountain west United States, 30; 1; 33-37.

7. Berardino Paolo, Fornaro Gianfranco, Lanari Riccardo, and S. Eugenio., 2002; A new algorithm for surface deformation monitoring based on small baseline differential SAR interferograms, IEEE Transactions on geoscience remote sensing; 40; 11; 2375-2383; 10.1109/TGRS.2002.803792.

8. Hooper Andrew, Segall P, and Zebker Howard, 2007; Persistent scatterer interferometric synthetic aperture radar for crustal deformation analysis, with application to Volcán Alcedo, Galápagos, Journal of Geophysical Research: Solid Earth; 112; B7; https://doi.org/10.1029/2006JB004763.

9. Hooper Andrew, Zebker Howard, Segall Paul, and K. Bert., 2004; A new method for measuring deformation on volcanoes and other natural terrains using InSAR persistent scatterers, Geophysical research letters 31; 23; https://doi.org/10.1029/2004GL021737.

10. Hooper, A., D.P.S. Bekaert, K. Spaans, and M. Arıkan, 2012; Recent advances in SAR interferometry time series analysis for measuring crustal deformation, Tectonophysics; 514-517; 1-13; 10.1016/j.tecto.2011.10.013.

11. Bui Luyen Khac, Featherstone WE, and F. MS, 2020; Disruptive influences of residual noise, network configuration and data gaps on InSAR-derived land motion rates using the SBAS technique, Remote Sensing of Environment; 247; 111941; https://doi.org/10.1016/j.rse.2020.111941.

12. Bui Khac Luyen , Le V.V. Phong, Dao Phuong Duc, Long Nguyen Quoc, Pham Hai Van, Tran Hong Ha, and X. Lei., 2021; Recent land deformation detected by Sentinel-1A InSAR data (2016–2020) over Hanoi, Vietnam, and the relationship with groundwater level change, GIScience Remote Sensing; 58; 2; 161-179; https://doi.org/10.1080/15481603.2020.1868198.

13. Long Nguyen Quoc, Van Anh Tran, Luyen Bui Khac, 2021; Determination of Ground Subsidence by Sentinel-1 SAR Data (2018-2020) over Binh Duong Quarries, Vietnam, VNU Journal of Science: Earth Environmental Sciences 37; 2; https://doi.org/10.25073/2588-1094/vnuees.4605.

14. Nam Bui Xuan, Van Anh Tran, Bui Luyen Khac, Long Nguyen Quoc, Ha Thi Le Thu, and G. Ropesh.; 2021; Mining-Induced Land Subsidence Detection by Persistent Scatterer InSAR and Sentinel-1: Application to Phugiao Quarries, Vietnam. in Proceedings of the International Conference on Innovations for Sustainable and Responsible Mining. Springer, 108; 18-38; http://doi.org/10.1007/978-3-030-60269-7_2.

15. Perski, Z., 1998; Applicability of ERS-1 and ERS-2 InSAR for land subsidence monitoring in the Silesian coal mining region, Poland, International Archives of Photogrammetry and Remote Sensing; 32; 555-558.

16. Krawczyk, A. and Z. Perski, 2000; Zastosowanie satelitarnej interferometrii radarowej na terenach eksploatacji rud miedzi w LGOM, XI Kongres ISM, Kraków.

17. Perski, Z., G. Ketelaar, and M.J.A.F. Mróz, Kartografii i Teledetekcji, 2006; Interpretacja danych Envisat/ASAR o przemiennej polaryzacji na obszarach zurbanizowanych w kontekście charakterystyki stabilnych rozpraszaczy (persistent scatterers), 16.

18. Perski Zbigniew, Hanssen Ramon, Wojcik Antoni, and W. Tomasz., 2009; InSAR analyses of terrain deformation near the Wieliczka Salt Mine, Poland, Engineering Geology; 106; 1-2; 58-67.

19. Wojciechowski, T., Z. Perski, and A.J.P.G. Wójcik, 2008; Wykorzystanie satelitarnej interferometrii radarowej do badań osuwisk w polskiej części Karpat, 56; 12; 1088-1091;

20. Graniczny Marek, Kowalski Zbigniew, Jureczka Janusz, and C. Magdalena.; 2006; Wykorzystanie technologii PSinSAR dla obserwacji przemieszczeń powierzchni terenu na przykładzie Górnego Śląska. in Mat. Symp. 127-129.

21. Malinowska, A., R. Hejmanowski, W.T. Witkowski, and A. Guzy, 2018; Mapping of slow vertical ground movement caused by salt cavern convergence with sentinel-1 tops data, Archives of Mining Sciences; 63; 2; 383-396; 10.24425/122453.

22. Mirek, K., 2009; Interferometric Synthetic Aperture Radar InSAR–method for study and monitoring subsidence over mining areas, Polish Journal of Environmental Studies; 18; 3A; 270.

23. Urbaniak, M.J.O.D.K., 2018; Kompleks młyna solnego i magazynów byłej kopalni soli w Wapnie. Uwarunkowania i przesłanki do ochrony XX-wiecznych budowli poprzemysłowych jako trwałej ruiny.

24. ttps://pl.wikipedia.org/wiki/Kopalnia_Soli_im._Tadeusza_Ko%C5%9Bciuszki_w_Wapnie; 28-07-2019 22:08 Wikipedia; Kopalnia Soli im. Tadeusza Kościuszki w Wapnie

25. Małachowski, K., 2018; The biggest surface mining disaster in Poland and its economic results, European Journal of Service Management; 28; 247-255; https://doi.org/10.18276%2Fejsm.2018.28%2F2-31.

26. https://plus.gloswielkopolski.pl/o-katastrofie-w-kopalni-soli-w-wapnie-nie-wolno-bylo-mowic-ani-pisac/ar/12399754; 19/8/2017 Dziuma, M.; O katastrofie w kopalni soli w Wapnie nie wolno było mówić ani pisać.

27. Tran, V. A., Bui, X. N., Nguyen, Q. L., & Tran, T. A. (2020). Land Subsidence Detection in Tan My-Thuong Tan Open Pit Mine and Surrounding Areas by Time Series of Sentinel-1 Images. Inżynieria Mineralna. DOI 10.29227/IM-2020-02-22

28. Chen, C.W. and H.A. Zebker, 2000; Network approaches to two-dimensional phase unwrapping: intractability and two new algorithms, Journal of the Optical Society of America A; 17; 3; 401-414; http://doi.org/10.1364/JOSAA.17.000401.